Cooperative Control of SFCL and SMES for Enhancing Fault Ride Through Capability and Smoothing Power Fluctuation of DFIG Wind Farm

Issarachai Ngamroo and Tanapon Karaipoom

***Abstract*—This paper deals with a cooperative control of a resistive type superconducting fault current limiter (SFCL) and a superconducting magnetic energy storage (SMES) for enhancing fault ride through (FRT) capability and smoothing power fluctuation of the doubly fed induction generator (DFIG)-based wind farm. When the system faults occur, the SFCL is used to limit the fault current, alleviate the terminal voltage drop, and transient power fluctuation so that the DFIG can ride through the fault. Subsequently, the remaining power fluctuation is suppressed by the SMES. The resistive value of the SFCL as well as the superconducting coil inductance of the SMES are simultaneously optimized so that a sudden increase in the kinetic energy in the DFIG rotor during faults, an initial stored energy in the SMES coil, an energy loss of the SFCL, and an output power fluctuation of the DFIG are minimum. The superior control effect of the cooperative SFCL and SMES over the individual device is confirmed by simulation study.**

***Index Terms*—Doubly fed induction generator (DFIG) wind turbine, optimization, superconducting fault current limiter (SFCL), superconducting magnetic energy storage (SMES).**

I. Introduction

RECENTLY, the doubly fed induction generator (DFIG)-based wind farms have been paid attentions extensively due to low cost of installation, controllable power output etc. [1]. Nevertheless, the DFIG faces two unavoidable problems, i.e., output power fluctuation and fault ride through (FRT) capability. The power fluctuation due to intermittent wind speeds may deteriorate power quality and system stability. Besides, the DFIG is vulnerable to the low voltage situation due to system faults. To protect the damage of the DFIG, the DFIG will be tripped from the system. The tripping of large wind farms may cause the system instability.

To overcome both problems, the superconducting magnetic energy storage (SMES) has been applied [2]–[4]. Since the SMES has no any effect on the fault current limitation, the enhancement of the FRT capability by the SMES may be degraded when severe faults are adjacent to the SMES location. On the other hand, the resistive type superconducting fault current limiter (SFCL) has been used to enhance the FRT capability of the DFIG wind turbine [5], [6]. Study results show that the higher the value of SFCL resistance, the better improvement of the FRT capability can be achieved. Nevertheless, the high resistance results in the high energy loss during the period of fault current limitation. Additionally, the resistance value of the SFCL in these works is selected based on trial-and-error which cannot guarantee the optimal value. The problems of the high energy loss and the optimal value of the resistance should be taken into account in the selection of the SFCL resistance.

To tackle all shortcomings above, the new optimization technique of the cooperative SFCL and SMES is proposed in this paper. SFCL and SMES models, optimization, and simulation results are described.

Manuscript received June 28, 2014; accepted July 14, 2014. Date of publication July 18, 2014; date of current version August 6, 2014. This work was supported by the King Mongkut's Institute of Technology Ladkrabang Research Fund.

The authors are with the School of Electrical Engineering, Faculty of Engineering, King Mongkut's Institute of Technology Ladkrabang, Bangkok 10520, Thailand (e-mail: ngamroo@gmail.com; krpoom@gmail.com).

Color versions of one or more of the figures in this paper are available online at http://ieeexplore.ieee.org.

Digital Object Identifier 10.1109/TASC.2014.2340445

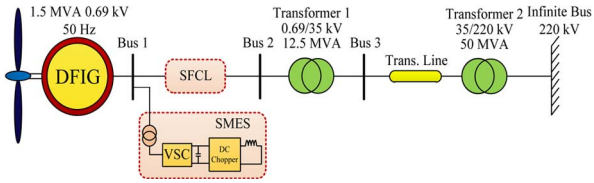

Fig. 1. DFIG wind turbine system with SFCL and SMES.

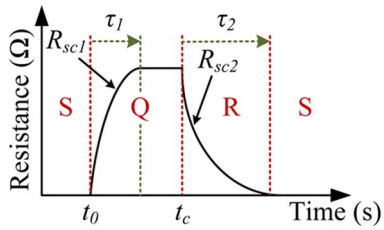

Fig. 2. Characteristic of resistive type SFCL.

II. Study System and Modeling

A. Study System

Fig. 1 shows the grid connected-DFIG wind turbine that is used as the study system [7]. The SMES and the resistive type SFCL are installed at the DFIG terminal bus 1.

B. Resistive Type SFCL Model

Fig. 2 depicts the characteristic of the resistive type SFCL which can be represented by a time-variant resistance [5], [8]. First, the SFCL is in a superconducting (S) state and the SFCL resistance is zero. At time $t = t_0$, the quenching (Q) state starts, the resistance of the SFCL increases exponentially by

$$R_{sc1}(t) = R_{m1}\left(1 - \exp(-t/\tau_1)\right), \tag{1}$$

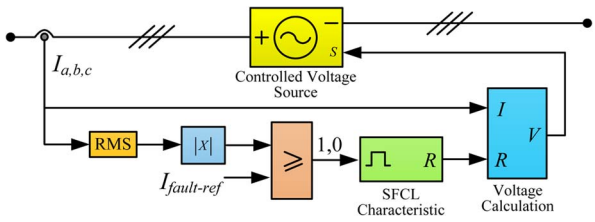

Fig. 3. SFCL model developed in MATLAB/SimPowerSystems.

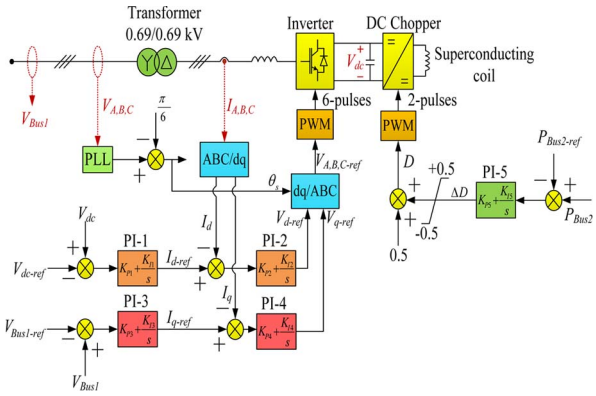

Fig. 4. SMES circuit and control system.

where $R_{sc1}(t)$ is the resistance of the SFCL from the superconducting state to the quenching state, R_{m1} is the maximum resistance, and τ_1 is the time constant of the quenching period. Subsequently, at $t = t_c$, the recovery (R) state starts and the SFCL resistance decreases exponentially by

$$R_{sc2}(t) = R_{m2}\left(1 - \exp(-t/\tau_2)\right), \tag{2}$$

where $R_{sc2}(t)$ is the value of SFCL resistance from the quenching state to the superconducting state, R_{m2} is the maximum resistance, and τ_2 is the time constant of the recovery period. Here, τ_1 and τ_2 are set at 1 ms and 50 ms, respectively. Since the quenching period and the recovery period are very short, this study assumes that $R_{m1} = R_{m2} = R_m$.

Fig. 3 shows the SFCL model developed in MATLAB/SimPowerSystems [9]. For the operation of this model, first three phase currents $(I_{a,b,c})$ are measured and used to calculate the RMS current. Subsequently, the RMS current is compared with the fault current reference $(I_{\text{fault-ref}})$. If the RMS current is greater than $I_{\text{fault-ref}}$, the signal "1" is sent to the SFCL characteristic block. As a result, the SFCL starts to operate. After that, the equivalent voltage drop across the resistance is calculated and sent to the controlled voltage source block. This equivalent voltage is injected to the AC line and shows the fault current limiting effect of the SFCL.

C. SMES Model

Fig. 4 shows the SMES circuit with the voltage source converter (VSC) control system. The SMES circuit is composed of capacitor, DC chopper, and superconducting coil with inductance (L_{SC}). Using the phase lock loop (PLL), the angle of the voltage transformation from three phase voltages (V_a, V_b, V_c) to $d-q$ axis voltages can be obtained. The VSC can be controlled by four proportional integral (PI) controllers. The first PI controller (PI-1) is used to generate the reference value of the direct axis current $(I_{d\text{-ref}})$ from the difference between the actual dc link voltage (V_{dc}) and the reference value of the dc link voltage $(V_{\text{dc-ref}})$. By comparing $I_{d\text{-ref}}$ and the actual current I_d, the obtained result is used as an input signal of the second PI controller (PI-2). After that, the reference value of the direct axis voltage $(V_{d\text{-ref}})$ is obtained from the output signal of PI-2.

In the same way, the reference value of the quadrature axis current $(I_{q\text{-ref}})$ is generated by the third PI controller (PI-3) which uses the difference between the actual voltage at bus 1 (V_{Bus1}) and the reference voltage at bus 1 $(V_{\text{Bus1-ref}})$ as an input signal. Subsequently, an input signal of the forth PI controller (PI-4) is obtained by the difference between $I_{q\text{-ref}}$ and the actual quadrature current (I_q). Consequently, the reference signal of the quadrature axis voltage $(V_{q\text{-ref}})$ is achieved as the output signal of PI-4. Both $V_{d\text{-ref}}$ and $V_{q\text{-ref}}$ are converted to three phase voltage references $(V_{A,B,C\text{-ref}})$. Comparing $V_{A,B,C\text{-ref}}$ with a triangular carrier waveform with 1980 Hz provides the gate drive signal of controlled switches in the VSC.

The PI-5 controller of DC chopper is used to control the exchange energy between the superconducting coil and the power system. The power error signal which is calculated from the difference between the actual power flow at bus 2 (P_{Bus2}) and the reference active power flow at bus 2 $(P_{Bus2\text{-ref}})$ is used as the input of PI-5. The output of the PI-5 is a duty cycle deviation (ΔD) which is added to the reference value $(+0.5)$ to get the duty cycle (D). The electrical energy is charged from the system to the SMES coil when D is greater than 0.5. The energy is discharged from the SMES coil to the system when D is less than 0.5.

In this study, R_m, L_{SC}, and ten PI parameters are simultaneously optimized.

III. Proposed Optimization

A. Optimization of SFCL

The SFCL optimization is conducted based on the suppression of the abrupt increase in the kinetic energy in the DFIG rotor during faults and the energy loss of the SFCL. As a result, not only the limitation of the fault current, but also the alleviation of the decrease in the terminal voltage and the power output can be obtained. The FRT capability enhancement of the DFIG can be expected.

As mentioned in [10], the first swings of the rotor angle and the rotor speed are minimum when the kinetic energy stored in the rotor during faults is minimized. The stored kinetic energy when the fault is cleared (E_K^f), can be expressed by

$$E_K^f = A(t_f - t_0)^2, \tag{3}$$

where

$$A = M\alpha^2/2, \tag{4}$$

where M is the inertia constant of DFIG rotor, t_0 is the time of the fault occurrence, t_f is the fault clearing time, α is the acceleration of the rotor during faults. The value of α can be approximated by

$$\alpha = (P_m - P_{ef})/M, \tag{5}$$

where P_m and P_{ef} are the mechanical power input and the electrical power output of DFIG at the time of the fault occurrence,

respectively. Here, instead of minimizing E_K^f, the minimization of A is carried out.

In addition, the energy loss of the SFCL during quenching state (E_{SFCL}) which is minimized, can be calculated by

$$E_{\mathrm{SFCL}} = \int_{t_0}^{t_f} i^2(t) R_m \, dt, \tag{6}$$

where $i(t)$ is the current flow through SFCL.

B. Optimization of SMES

After the operation of the SFCL, the SMES is used to eliminate the unbalanced kinetic energy so that the remaining power fluctuation can be suppressed. Besides, during normal operation, the SMES is used to alleviate the output power fluctuation of the DFIG. Here, the minimization of the integral absolute error (IAE) of the power deviation at bus 2 $(\Delta P_{\mathrm{Bus2}})$ is considered by

$$IAE = \int_{t_i}^{t_s} |\Delta P_{Bus2}| \, dt, \tag{7}$$

where t_i and t_s are the initial time and the final time of simulation.

The initial stored energy of the SMES is determined by

$$E_{SC0} = L_{SC} I_{SC0}^2 / 2, \tag{8}$$

where E_{SC0} is the initial stored energy of SMES, and I_{SC0} is the initial coil current. Here, L_{SC} and I_{SC0} are optimized so that the initial stored energy is sufficient for achieving all objectives.

C. Formulation of Optimization Problem of SFCL and SMES

Combining (4), (6), (7), and (8), the optimization problem of SFCL and SMES can be formulated by

$$\begin{aligned}
&\text{Minimize } A + E_{\mathrm{SFCL}} + IAE + E_{SC0} \\
&\text{Subject to} \\
&\text{(a)} \quad 0.01 \le R_m \le 2\ \Omega \text{ (range of SFCL resistance)} \\
&\text{(b)} \quad 0.001 \le L_{SC} \le 5\ \text{H (range of SMES coil inductance)} \\
&\text{(c)} \quad 0.1 \le I_{SC0} \le 5\ \text{kA (range of SMES initial coil current)} \\
&\text{(d)} \quad 0.0001 \le K_{P1}, K_{P2}, K_{P3}, K_{P4}, K_{P5} \\
&\qquad \le 5 \text{ (range of } K_P \text{ gains)} \\
&\text{(e)} \quad 0.0001 \le K_{I1}, K_{I2}, K_{I3}, K_{I4}, K_{I5} \\
&\qquad \le 10 \text{ (range of } K_I \text{ gains).}
\end{aligned} \tag{9}$$

The control effect of the optimized SFCL and SMES is compared with the optimized SFCL or the optimized SMES.

The optimized parameters of the SFCL is conducted by

$$\begin{aligned}
&\text{Minimize } A + E_{\mathrm{SFCL}} \\
&\text{Subject to constraints (a).}
\end{aligned} \tag{10}$$

The optimized parameters of the SMES is carried out by

$$\begin{aligned}
&\text{Minimize } IAE + E_{SC0} \\
&\text{Subject to constraints (b), (c), (d), and (e).}
\end{aligned} \tag{11}$$

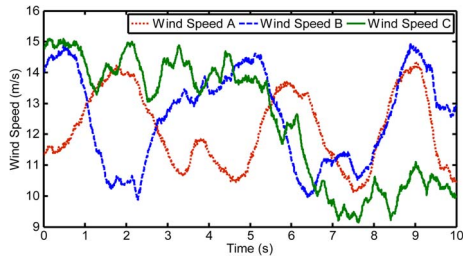

Fig. 5. Wind speed patterns.

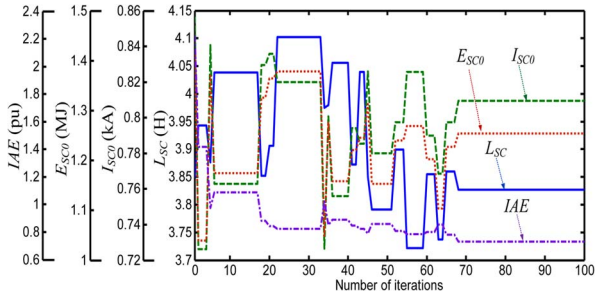

Fig. 6. Convergence curves of IAE, E_{SC0},I_{SC0}, and L_{SC}.

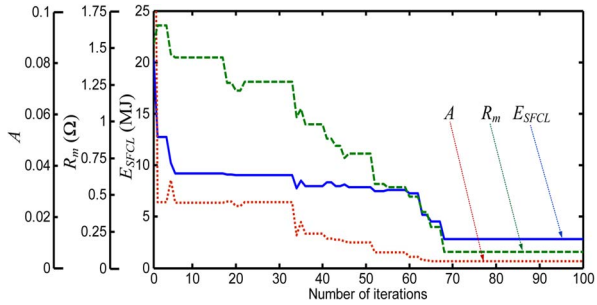

Fig. 7. Convergence curves of A, R_m, and E_{SFCL}.

The particle swarm optimization [11] is used to achieve all optimal parameters.

IV. Simulation Study

The optimization is carried out under the wind speed pattern A as shown in Fig. 5 and a temporary three phase fault at bus 3 at $t = 3$ s for 150 ms. After the optimization, Figs. 6 and 7 show the convergence curves of IAE, E_{SC0}, I_{SC0}, and L_{SC} as well as those of A, R_m, and E_{SFCL}, respectively. The optimized parameters of all devices are given in Table I. It can be observed that the resistance and the energy loss of the SFCL in case of the SFCL and SMES are lower than those in case of the SFCL. Additionally, the inductance and the initial stored energy of the SMES in case of the SFCL and SMES are lower than those in case of the SMES.

First, the power smoothing effect of the SMES is evaluated under three patterns of the wind speed in Fig. 5. Fig. 8 shows the active power output of the DFIG in case the wind speed A. Fig. 9 depicts the IAE of the power output deviation at bus 2 with respect to three wind patterns. Without any device, the power at bus 2 drastically fluctuates. It can be seen that the SFCL has no any effect on the alleviation of power fluctuation because the SFCL is not able to exchange the energy with the power systems. On the other hand, the SFCL and SMES as well as the SMES are able to alleviate the power fluctuation

TABLE I
OPTIMIZED PARAMETERS OF SFCL AND SMES

Parameters	SFCL	SMES	SFCL and SMES
R_m (Ω)	0.165	-	0.112
E_{SFCL} (MJ)	4.058	-	2.812
L_{SC} (H)	-	4.521	3.827
I_{SC0} (kA)	-	0.826	0.809
E_{SC0} (MJ)	-	1.542	1.252
K_{P1}, K_{I1}	-	4.834, 2.123	2.120, 4.586
K_{P2}, K_{I2}	-	0.367, 6.993	4.103, 7.179
K_{P3}, K_{I3}	-	2.716, 5.090	0.833, 4.592
K_{P4}, K_{I4}	-	0.489, 4.838	0.496, 4.815
K_{P5}, K_{I5}	-	2.971, 5.079	3.092, 0.043

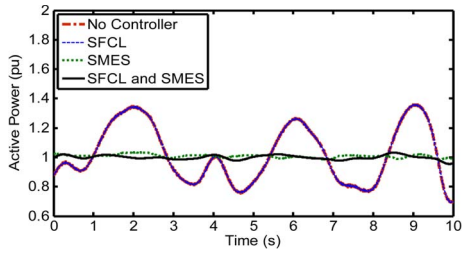

Fig. 8. Active power flow at bus 2 (Wind speed A).

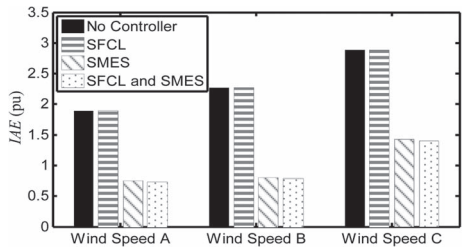

Fig. 9. IAE of power deviation at bus 2.

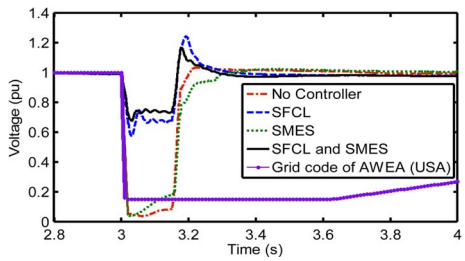

Fig. 10. Terminal voltage of DFIG at bus 1.

effectively. The IAE in case of the SFCL and SMES is almost the same as that in case of the SMES.

Next, the time simulation under a temporary three phase fault at bus 3 at $t = 3$ s for 150 ms is conducted to evaluate the improvement of the FRT capability by the SFCL and SMES. According to the grid code of USA AWEA, the wind turbine must withstand 15% of voltage dip at the connection point with duration of up to 625 ms [12]. Fig. 10 shows the terminal voltage of the DFIG at bus 1. The voltage dips in case of without any device as well as with the SMES are lower than the minimum acceptable voltage of the grid code. This indicates that the DFIG cannot ride through the fault. On the other hand, in case of the SFCL as well as the SFCL and SMES, the voltage dips are still in the acceptable range of the grid code.

TABLE II
NECESSARY MW AND MJ CAPACITIES OF SMES

Capacity	SMES	SMES-FCL
MW	3.561	1.609
MJ	8.06	7.778

Nevertheless, the SFCL and SMES provide better control effect than the SFCL. The cooperative control of SFCL and SMES not only suppresses the transient voltage effectively, but also eliminates the following voltage fluctuation entirely.

Table II shows the comparison results of necessary MW and MJ capacities of the SMES under the applied fault. The MW capacity is calculated from the maximum power output of the SMES. The MJ capacity is determined from the difference between the maximum and the minimum energy outputs of theSMES. With the contribution of the SFCL, necessary MW and MJ capacities of SMES are less than those in case of the only SMES.

V. CONCLUSION

The cooperative control of SFCL and SMES for augmenting FRT capability and suppressing power fluctuation of the DFIG wind turbine is proposed. The parameters optimization of SFCL and SMES is automatically conducted to achieve the desired objectives. Study results confirm that the cooperative SFCL and SMES not only provide superior control effect than the individual device, but also reduce the power and energy capacities of SMES.

REFERENCES

[1] G. Abad, J. Lopez, M. Rodriguez, L. Marroyo, and G. Iwanski, *Doubly Fed Induction Machine: Modeling and Control for Wind Energy Generation*. Hoboken, NJ, USA: Wiley, 2011.
[2] J. Shi, Y. J. Tang, L. Ren, J. D. Li, and S. J. Chen, "Application of SMES in wind farm to improve voltage stability," *Physica C, Supercond.*, vol. 468, no. 15–20, pp. 2100–2103, Sep. 2008.
[3] S.-T. Kim, B.-K. Kang, S.-H. Bae, and J.-W. Park, "Application of SMES and grid code compliance to wind/photovoltaic generation system," *IEEE Trans. Appl. Supercond.*, vol. 23, no. 3, p. 5000804, Jun. 2013.
[4] A. M. S. Yunus, M. A. S. Masoum, and A. Abu-Siada, "Application of SMES to enhance the dynamic performance of DFIG during voltage sag and swell," *IEEE Trans. Appl. Supercond.*, vol. 22, no. 4, p. 5702009, Aug. 2013.
[5] W.-J. Park, B. C. Sung, and J.-W. Park, "The effect of SFCL on electric power grid with wind-turbine generation system," *IEEE Trans. Appl. Supercond.*, vol. 20, no. 3, pp. 1177–1181, Jun. 2010.
[6] M. E. Elshiekh, D. A. Mansour, and A. M. Azmy, "Improving fault ride-through capability of DFIG-based wind turbine using superconducting fault current limiter," *IEEE Trans. Appl. Supercond.*, vol. 23, no. 3, p. 5601204, Jun. 2013.
[7] W. Guo, L. Xiao, and S. Dai, "Enhancing low-voltage ride-through capability and smoothing power output of DFIG with a superconducting fault-current limiter-magnetic energy storage system," *IEEE Trans. Energy Convers.*, vol. 27, no. 2, pp. 277–295, Jun. 2012.
[8] K. Hongesombut, Y. Mitani, and K. Tsuji, "Optimal location assignment and design of superconducting fault current limiters applied to loop power systems," *IEEE Trans. Appl. Supercond.*, vol. 13, no. 2, pp. 1828–1831, Jun. 2003.
[9] MATLAB SimPowerSystems, New York, NY, USA: Mathworks, 2014.
[10] P. Kundur, *Power System Stability and Control*. New York, NY, USA: McGraw-Hill, 1994.
[11] J. Kennedy, "Particle swarm optimization," in *Proc. IEEE Int. Conf. Neural Netw.*, Nov. 1995, pp. 1942–1948.
[12] J. Schlabbach, "Low voltage fault ride through criteria for grid connection of wind turbine generators," in *Proc. 5th Int. Conf. Eur. Elect. Market*, 2008, pp. 1–4.